Slow spatial migration can help eradicate cooperative antimicrobial resistance in time-varying environments

Lluís Hernández-Navarro[1,†,*], Kenneth Distefano[2,†], Uwe C. Täuber[2,3], and Mauro Mobilia[1,*]

[1]Department of Applied Mathematics, School of Mathematics, University of Leeds, Leeds LS2 9JT, U.K.

[2]Department of Physics & Center for Soft Matter and Biological Physics, MC 0435, Robeson Hall, 850 West Campus Drive, Virginia Tech, Blacksburg, VA 24061, USA

[3]Faculty of Health Sciences, Virginia Tech, Blacksburg, VA 24061, USA

[†]These authors contributed equally to this work

*L.Hernandez-Navarro@leeds.ac.uk, M.Mobilia@leeds.ac.uk

February 12, 2025

Abstract

Antimicrobial resistance (AMR) is a global threat and combating its spread is of paramount importance. AMR often results from a cooperative behaviour with shared drug protection. Microbial communities generally evolve in volatile, spatially structured settings. Migration, fluctuations, and environmental variability significantly impact AMR. While AMR is enhanced by migration in static conditions, this changes in time-fluctuating spatially structured environments. We consider a two-dimensional metapopulation consisting of demes in which drug-resistant and sensitive cells evolve in a time-changing environment containing a toxin against which protection can be shared. Cells migrate between demes and connect them. When the environment varies neither too quickly nor too slowly, population bottlenecks cause fluctuation-driven extinctions, countered by migration. We investigate the influence of migration and environmental variability on AMR, determining the near-optimal conditions for resistance eradication. We show how slow migration

speeds up and enhances AMR clearance. We discuss our study's impact on laboratory-controlled experiments.

Author summary

As the number of microbes resisting antimicrobial drugs grows alarmingly, it is of paramount importance to tackle this major societal issue. Resistant microbes often inhibit antibiotics in the environment around them, and hence offer protection to drug-sensitive bacteria in a form of cooperative behaviour. Moreover, microbes typically are distributed in space and live in time-changing environments, where they are subject to random fluctuations. Environmental variability, fluctuations, and spatial dispersal all have a strong influence on the drug resistance of microbial organisms. Here we investigate the evolution of antimicrobial resistance in time-varying spatial environments by combining computational and mathematical means. We study the dynamics of drug-resistant and sensitive cells in the presence of an antimicrobial drug, when microbes are spatially distributed across a two-dimensional grid of well-mixed sub-populations (demes). Cells migrate between neighbouring demes, connecting these sub-populations, and are subject to sudden changes of environment. We show that when environmental variations occur neither too rarely nor too often, the joint effect of slow migration and fluctuations can help eradicate drug resistance by speeding up and enhancing the extinction probability of resistant bacteria. We also discuss how our findings can be probed in laboratory experiments.

1 Introduction

Microbial communities generally live in volatile, time-varying environments embedded in complex spatial structures connected through cellular migration, e.g., in soil [1], seabed [2], on wet surfaces [3], in plants [4], animals [5], and humans [6, 7]. How the environment helps shape microbial populations and species diversity [8, 9, 10, 11] is a subject of intense research [11, 12, 13, 14, 15, 16, 17, 18, 19, 20, 21, 22]. Moreover, environmental variability and microbiome-environment interactions greatly influence the evolution of microbial communities, with a growing interest in their eco-evolutionary dynamics [6, 10, 22, 23, 24, 25, 26, 27, 28]. Despite significant recent progress [13, 14, 21, 22], a general understanding of the joint influence of spatial structure and environmental variability on the evolution of microbial populations remains an open question that is notably relevant to the spread of antimicrobial resistance (AMR) [29, 30, 31]. The evolution of AMR is of paramount societal importance, and is influenced by spatial structure, environmental changes and fluctuations. The latter are often associated with population bottlenecks [10], when the community size is drastically reduced,

e.g., due to the effects of a drug [32, 33] or to other causes [34, 35]. The size and composition of microbial populations are often interdependent, leading to coupled environmental and demographic fluctuations [23, 26, 27, 28, 36, 37, 38, 39, 40, 41]. These are particularly relevant when antibiotics cause bottlenecks following which surviving cells may replicate and AMR can spread [33]. Recent studies have investigated the impact of space on the emergence and spread of non-cooperative AMR mutants [11, 15], even in the presence of environmental bottlenecks [20, 22]. However, AMR often results from cooperative behaviour with resistant microbes inactivating toxins and sharing their protection with drug-sensitive bacteria [21, 35, 42]. Recent research on cooperative AMR has mostly focused on microbiome-environment interactions [14, 21], without considering external environmental changes.

Here, inspired by β-lactamase cooperative AMR [35, 42, 43], we study how the migration of cells shapes the evolution of AMR in a spatially structured microbial population subject to environmental variability causing bottlenecks and fluctuations. To this end, we investigate the *in silico* evolution of cooperative antimicrobial resistance in a two-dimensional (2D) metapopulation consisting of cells that are either sensitive (S) or resistant (R) to a drug. In this explicit spatial model, the microbial community consists of a grid of linear size L, containing $L \times L$ demes whose well-mixed sub-populations are connected by cell migration (at a rate m), and is subject to a constant antimicrobial input and a time-fluctuating environment. We model environmental variability by letting the carrying capacity of each deme, $K \in \{K_-, K_+\}$, randomly switch back and forth between $K = K_+$, when the environment is mild, and $K = K_- < K_+$ under harsh conditions, across the entire metapopulation at frequencies ν_+ and ν_- (Fig. 1a). Whenever the number N_R of R cells in a deme exceeds a cooperative threshold N_{th}, the protection against the drug becomes a public good and is shared with all the N_S sensitive bacteria in that deme, whereas the number of cells in each deme fluctuates with K (Fig. 1b). In this setting, we investigate how cell migration and environmental fluctuations influence the evolution of antimicrobial resistance, and under which circumstances all resistant cells can be eradicated from the entire metapopulation.

2 Results

2.1 Bottlenecks can cause resistance fluctuation-driven eradication in isolated demes

It is useful to first address the evolution of R and S cells in a single isolated deme (Fig. 1a). When the environment varies either very quickly or slowly compared to the intra-deme dynamics, the eradication of R cannot be observed as resistant cells generally survive for extended periods [26] (Methods and

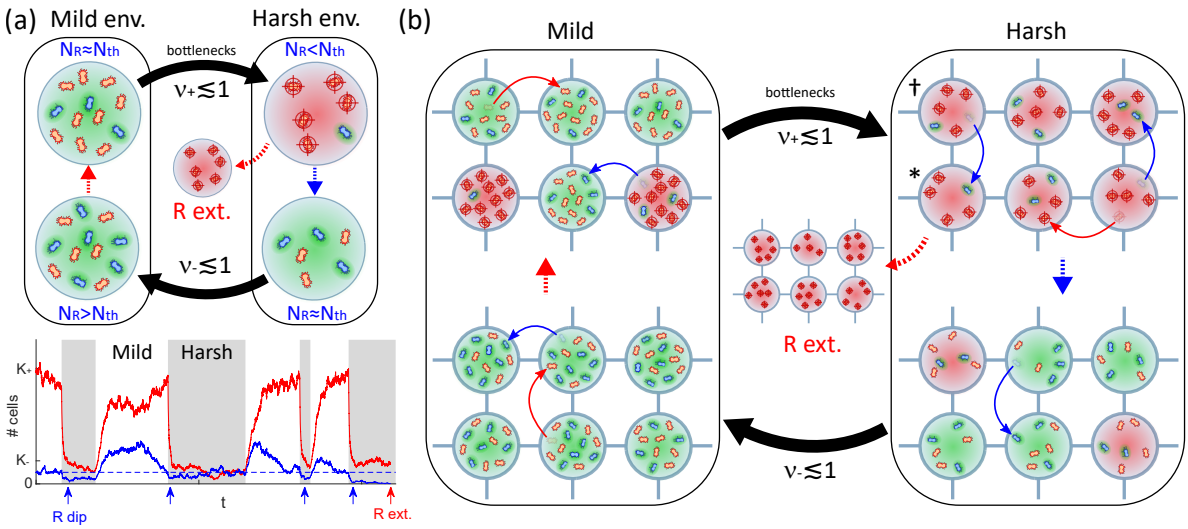

Figure 1: **Microbial community model.** **(a)** Eco-evolutionary dynamics in one isolated deme ($m = 0$) at constant antimicrobial input and intermediate environmental switching (Methods). **Top.** Illustrative evolution when the environment switches between mild (carrying capacity $K_+ = 12$) and harsh ($K_- = 6$) conditions at rates $\nu_\pm \lesssim 1$ (Supplementary Figure 1 and Supplementary Section 3), with cooperation threshold $N_{\rm th} = 3$. Each resistant microbe (blue, R) produces a resistance enzyme that locally inactivates the drug (green shade) at a metabolic cost reducing their growth rate. When the number of R cells exceeds the threshold, $N_R \geq N_{\rm th}$, the drug is inactivated in the entire deme and sensitive cells (red, S) benefit from the shared protection at no cost (bottom-left green shade, public good), which increases the S fraction (upward red arrow). When $N_R < N_{\rm th}$, the drug is active (red shade, top-right) and the spread of S cells is hampered (red crosshairs) while R are protected and thrive (downward blue arrow). If $N_R > N_{\rm th}$ in the mild environment (left black box, $K = K_+$), the R population decreases towards the cooperation threshold, $N_R \to N_{\rm th}$, whereas the S population approaches $K_+ - N_{\rm th}$ (upward arrow). Similarly, if $N_R < N_{\rm th}$ in the harsh environment (right box, $K = K_-$), the number of R increases to $N_R \to N_{\rm th}$ while $N_S \to K_- - N_{\rm th}$ (downward arrow). To model environmental volatility, we assume that K switches suddenly between K_+ and K_-, driving the deme population size ($N = N_S + N_R$). At intermediate switching, when $\nu_\pm \lesssim 1$, the population experiences bottlenecks whenever the environment changes from mild ($K = K_+$) to harsh ($K = K_-$). When $K_+/K_- \gtrsim N_{\rm th}$ [26] (Methods), demographic fluctuations may cause the extinction of R cells after each bottleneck (curved dashed red arrow). **Bottom.** Stochastic realisation of N_S (red curve) and N_R (blue) in a deme vs. time (Methods), with parameters $N_{th} = 40$ (dashed line), $K_+ = 400$, $K_- = 80$, $\nu_+ = 0.075$, and $\nu_- = 0.125$. White/grey background indicates mild/harsh environment. Population bottlenecks (white-to-grey) enforce transient N_R dips (blue arrows) promoting fluctuation-driven R eradication (red arrow). **(b)** Eco-evolutionary metapopulation dynamics; legend and parameters are as in (a). The metapopulation is structured as a two-dimensional grid (periodic boundary conditions) of connected demes, all at carrying capacity $K(t) \in \{K_-, K_+\}$. Each R and S cell can migrate onto a neighbouring deme at rate m (curved coloured arrows, Methods). Owed to local N_R fluctuations, drug inactivation varies across demes (different shades). Population bottlenecks can locally eradicate R, e.g. in deme ($*$), but migration from a neighbouring deme ($\dagger$) can rescue resistance (curved blue arrow). Resistance is fully eradicated when no R cells survive across the entire grid (curved dashed red arrow).

Supplementary Section 2). Here, we focus on environments varying at an intermediate switching rate, neither too fast nor too slow, allowing the size of a deme to track the switching carrying capacity (Fig. 8a and Methods, Supplementary Fig. 1), and assume $N_{\rm th} < K_- < K_+$. In this biologically relevant regime [44, 45], when the environment switches from mild to harsh and the carrying capacity from K_+ to K_-, the population experiences bottlenecks, and demes contain generally more S bacteria than R cells (blue arrows in the sample paths of Fig. 1a (bottom), Supplementary Movies can be found at the OSF data repository osf.io/epb28, see Data availability section, with full description

of the movies in the Supplementary Information Section 3). Henceforth, we quantify the bottleneck strength as K_+/K_-, which also serves as a measure of environmental variability. We have demonstrated that in intermediate-switching environments, in a well-mixed population subject to strong bottlenecks (large K_+/K_-), fluctuations cause the extinction of R cells when $K_+/K_- \gtrsim N_{\text{th}}$ on an average time $4/(\nu_+ + \nu_-)$ (Fig. 1a bottom, Methods) [26]. This phenomenon where resistance is cleared by the coupled effect of environmental and demographic fluctuations is called "fluctuation-driven eradication" (Methods). In this work, we investigate under which conditions this resistance eradication mechanism can hold in a two-dimensional metapopulation. This is an important and intriguing question since microbial communities generally evolve in spatial settings, and locally R-free demes can be recolonized by cells migrating from neighbouring sites (migration from cross to asterisk deme in Fig. 1b). Migration is thus expected to generally favour the coexistence of R and S cells across the metapopulation (Fig. 8d, Supplementary Fig. 2 and Supplementary Section 2), and more generally promotes bacterial diversity [46]. However, we show that fluctuation-driven eradication also occurs on the 2D grid and unveils an intriguing regime where migration even enhances this phenomenon of resistance clearance.

2.2 Critical migration rate and bottleneck strength to eradicate antimicrobial resistance

To study the eradication of resistance in the 2D metapopulation, we focus on the regime of intermediate environmental switching and moderate/slow migration, where $0 < m \lesssim 1$. This corresponds to each deme experiencing bottlenecks with a frequency of order $(\nu_+ + \nu_-)/4$, leading to local R eradication in a time scaling with $1/(\nu_+ + \nu_-)$ (Fig. 1a bottom and Methods), and single cells migrating between nearest-neighbour sites on a similar or slower time scale (Figs. 2 and 3). This results in demes being neither entirely isolated ($m = 0$), nor all fully connected (fast migration, $m \gg 1$), and spatial structure shaping the microbial dynamics. Since any R-free deme can be recolonised by resistant cells migrating in (Fig. 1b), it is not obvious whether eradication of resistance can arise in the spatial metapopulation. We find that environmental conditions causing strong bottlenecks, i.e. larger K_+/K_- values, increase the chances of clearing resistance across all demes (red/dark phase in Figs. 2a and 7). This effect is countered by fast migration: when m is increased and many cells migrate between two consecutive bottlenecks, the fluctuation-driven eradication of R cells is severely suppressed (white/light phase in Figs. 2a, 4, and 7). Remarkably, there is a trade-off between these contrasting effects, and we have determined the minimum bottleneck strength K_+/K_- and maximum migration rate m_c for which fluctuations can clear resistance across the whole metapopulation in a finite time (border between dark-red and light phases in Fig. 2a, see Fig. 2b-j). The critical migration rate m_c can be estimated

by matching the number of R migration events between two successive bottlenecks with the number of new R-free demes in each bottleneck. In the intermediate switching regime, this argument yields (Methods)

$$m_c \simeq \frac{\nu_+ \nu_-}{2\nu N_{\text{th}} \left(\exp\{ \frac{N_{\text{th}} K_-}{K_+} \} - 1 \right)}, \tag{1}$$

where $\nu = (\nu_- + \nu_+)/2$ is the average switching rate. This analytical prediction approximately captures the border between the red/white phases and how m_c increases with K_+/K_- in a biologically relevant regime (green lines in Fig. 2a and Fig. 4a-e). The fluctuation-driven eradication of R across the 2D metapopulation hence requires intermediate environmental switching, strong enough bottlenecks, and slow to moderate migration, which can be summarised by (Figs. 2a, 4, and 7; Methods):

$$\nu \lesssim 1, \quad \frac{K_+}{K_-} \gtrsim N_{\text{th}} \quad \text{and} \quad m \lesssim m_c. \tag{2}$$

These conditions are valid when the bottleneck frequency is comparable to the rate of change of the deme composition (Methods). Furthermore, we have found that very strong bottlenecks, $K_+/K_- \gtrsim N_{\text{th}} L^2$, can eradicate R from all demes at once, regardless of the migration rate (Methods). Moreover, when there are fewer single cell migrations between two successive bottlenecks than demes in the metapopulation, migration is effectively irrelevant (equal red levels for $m \in [0, 10^{-3.5}]$ in Fig. 2a and for $m \in [0, 10^{-4.5}]$ in Fig. 4a-e; Methods).

2.3 Breaking it down: bottlenecks and fluctuations vs. spatial mixing

To understand the joint influence of bottlenecks and migration on R eradication, we analyse the typical time evolution of the metapopulation subject to intermediate switching and migration rates, with moderate bottleneck strength (Fig. 3, where $K_+/K_- = 25$, Supplementary Section 3 Movie 3). The microbial composition of a single deme fluctuates due to environmental switches and random birth-death events, until demographic fluctuations eventually lead to R eradication in the deme (Fig. 3a). This resistance clearance mechanism, driven by bottlenecks and fluctuations, occurs randomly across the 2D grid (scattered red sites in Fig. 3e). However, R cells can randomly migrate from neighbouring demes and recolonise resistant-free sites (Fig. 3b). Recolonisation can spread in space, favouring microbial coexistence (pink clusters in Fig. 3e-f). Hence, the occurrence of bottlenecks increases the fraction of R-free demes across the grid (one spike for each bottleneck of Fig. 3d), whereas recolonisation reduces the fraction of S-only sites, leading to decays following bottleneck-induced spikes (Fig. 3d). Spikes are higher the stronger the bottlenecks, i.e. larger K_+/K_-, while the decreases steepen for faster migration, i.e. faster migration rates m (Fig. 2b-j and Methods). In the example of Fig. 3, the

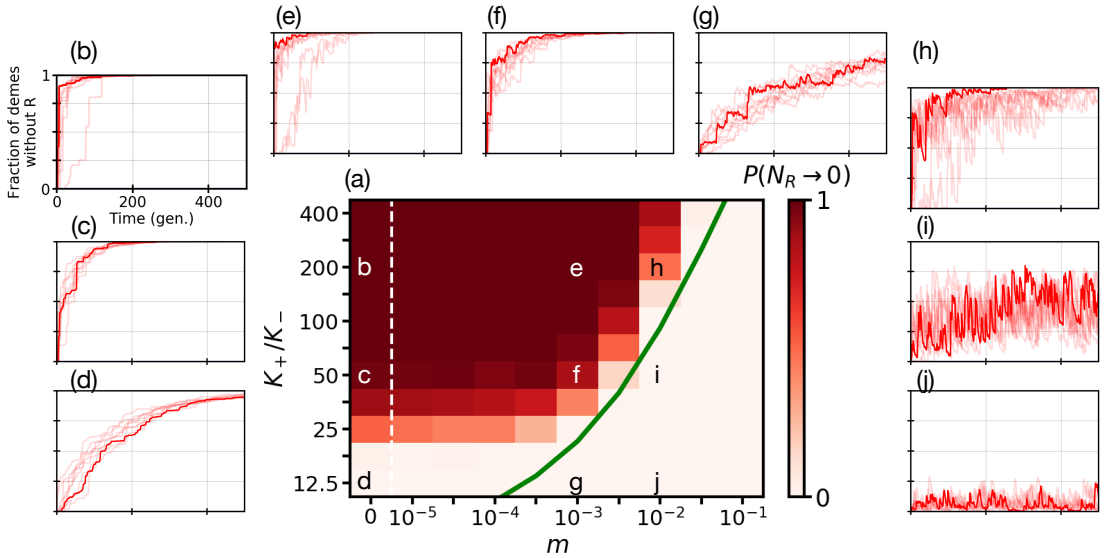

Figure 2: **The eradication mechanism of R cells depends on the bottleneck strength and migration rate.** The shared parameters in all panels are $\nu = 1$, $\delta = 0.75$, $L = 20$, $a = 0.25$, $s = 0.1$, $N_{\text{th}} = 40$, and $K_- = 80$ (Methods) with migration according to (7). Other parameters are as listed in Table 1 (Methods). **(a)** Heatmap of he probability of total extinction of R (resistant) cells, $P(N_R \to 0)$, as a function of bottleneck strength, K_+/K_-, and migration rate m. Each $(m, K_+/K_-)$ value pair represents an ensemble average of 200 independent simulations, where we show the fraction of realisations resulting in complete extinction of R (resistant) microbes, given by $P(N_R \to 0)$, after running each realisation for 500 microbial generations (Methods). The colour bar ranges from light to dark red, where darkest red indicates that complete extinction of R was found in all 200 simulations, $P(N_R \to 0) = 1$. The green line is the theoretical prediction of Eq. (1) (Discussion and Methods) and the white dashed vertical line indicates an axis break separating $m = 0$ and $m = 10^{-5}$ (Methods). The black and white annotated letters point to the specific $(m, K_+/K_-)$ values used in the outer panels. **(b-j)** Typical example trajectories of the fraction of demes without R cells (fixation of sensitive cells) as a function of time (microbial generations) for several specific $(m, K_+/K_-)$ values as indicated in panel (a). One example trajectory out of ten is marked in bright red for visualization purposes.

number of R-free demes steadily increases with the number of bottlenecks and, migration not being fast enough to rescue resistance in sufficient sites, R cells are eventually eradicated across the whole metapopulation (more red in Fig. 3g-h than in Fig.3e-f; fraction of R-free demes approaches one in Fig. 3d; Supplementary Section 3 Movie 3).

2.4 Slow migration can speed up and enhance resistant cells' eradication

We have disentangled the trade-off between the population bottleneck strength K_+/K_- and the migration rate m. To further clarify the interplay between fluctuations and migration in the 2D metapopulation, we investigate how this trade-off depends on m and K_+/K_- over time, and how it changes for different values of the switching rate (Figs. 4 and 7, Supplementary Fig. 3). Under the conditions (2), the overall resistance eradication probability increases in time (Fig. 4a-e): the R eradication mechanism overcomes microbial mixing, and the red phase expands in time until it reaches its border where $m \approx m_c$ (Eqs. (1) and (2); Methods). Remarkably, R cells in Fig. 4 are most likely to be eradicated from the metapopulation under slow but non-zero migration (red regions in Fig. 4c-e at

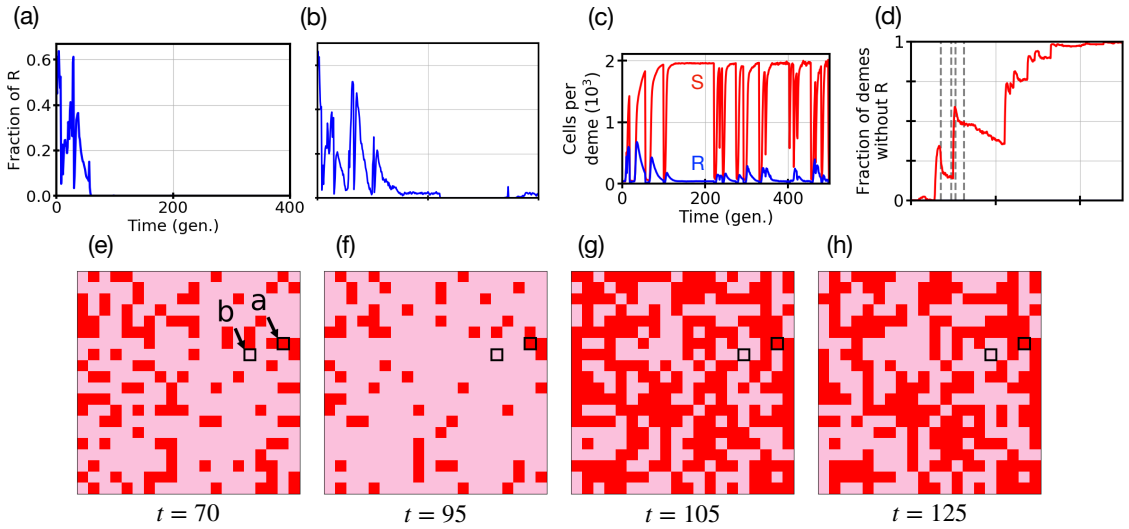

Figure 3: **A closer look to individual demes: migration and intermediate environmental switches shape local eradication of R cells.** Example eco-evolutionary dynamics of a single metapopulation. Parameters are $K_+ = 2000$, $\nu = 0.1$, $\delta = 0.5$, and $m = 0.001$, with density-dependent migration according to (7) (Supplementary Section 3, Movie 3); other parameters are as in Table 1 (Methods). **(a-b)** Evolution of the R (resistant) fraction in two example demes; see highlighted pixels in panels (e-h). The deme of panel (a) first shows coexistence, followed by fluctuation-driven R eradication due to environmental bottlenecks. In panel (b), the same dynamics is followed by recovery of R cells through recolonisation, as indicated by the blue spikes at long times (Discussion). **(c)** Evolution of the number of S and R cells in demes with both types (pink pixels in panels (e-h)). In fluctuation-driven eradication regimes, these demes consist of a majority of S cells ($N_{\text{th}} < K_- \ll K_+$). Subsequent bottlenecks cause sharp dips in the R and S populations, following which demographic fluctuations can drive R cells to local extinction. **(d)** Evolution of the fraction of demes without R cells (red pixels within panels (e-h)). From left to right, the dashed vertical lines indicate the corresponding snapshot times in panels (e-h). **(e-h)** Snapshots of the metapopulation of 20×20 demes at four microbial generation times $t \in \{70, 95, 105, 125\}$. Red pixels indicate R-free demes (only S cells are present) and pink pixels show demes with both cell types. The two demes of interest corresponding to panels (a-b) are indicated by a black border. Panel (e) shows the metapopulation a few generations after an environmental bottleneck. From panels (e) to (f) no bottleneck occurs, and many S-only demes are recolonised by R cells migrating in (many red pixels become pink). Then, between panels (f) and (g), the metapopulation experiences a bottleneck that causes a burst of local, single-deme R extinctions (burst of red pixels at random locations in panel (g), spike in the number of R-free demes of panel (d)). Again, expanding pink clusters are shown between panels (g) and (h) due to many R recolonisations after 20 generations (without environmental bottlenecks). Supplementary Section 3 Movie 3 shows the full spatial metapopulation dynamics for this example realisation.

$m \sim 10^{-4} - 10^{-3}$ darker than at $m \sim 0 - 10^{-4.5}$; Supplementary Section 3 Movies 1-2). The probability of R eradication (S fixation) thus rapidly increases and plateaus near 1 for $m \sim 10^{-4} - 10^{-3}$ (Fig. 4f): for these migration rates, which are comparable to those realised in microfluidic experiments [47], the clearance of resistance is almost guaranteed. Furthermore, we have studied the R eradication probability as function of K_+/K_- and m for a range of slow, intermediate and fast switching rates ν, confirming that R eradication occurs chiefly for $0.1 \lesssim \nu \lesssim 1$ (Fig. 7 and Supplementary Fig. 3).

These results demonstrate that not only does fluctuation-driven eradication of the resistant strain R arise in the 2D metapopulation under the conditions (2), but that slow migration ($0 < m < m_c$) actually *speeds up* the clearance of resistance and it *can even enhance* the probability of R eradication

(Methods and Supplementary Section 3 Movie 2). When resistant cells randomly take over a deme during periods in the harsh environment, with the low carrying capacity $K = K_-$ (blue in Fig. 6c,e, Supplementary Sections 2-3 and Movie 1), the fluctuation-driven eradication mechanism does not work on this deme in isolation any more. However, slow migration rates allow sensitive cells to recolonise the deme and make it susceptible to R eradication (Methods and Fig. 8, Supplementary Section 3 Movie 2).

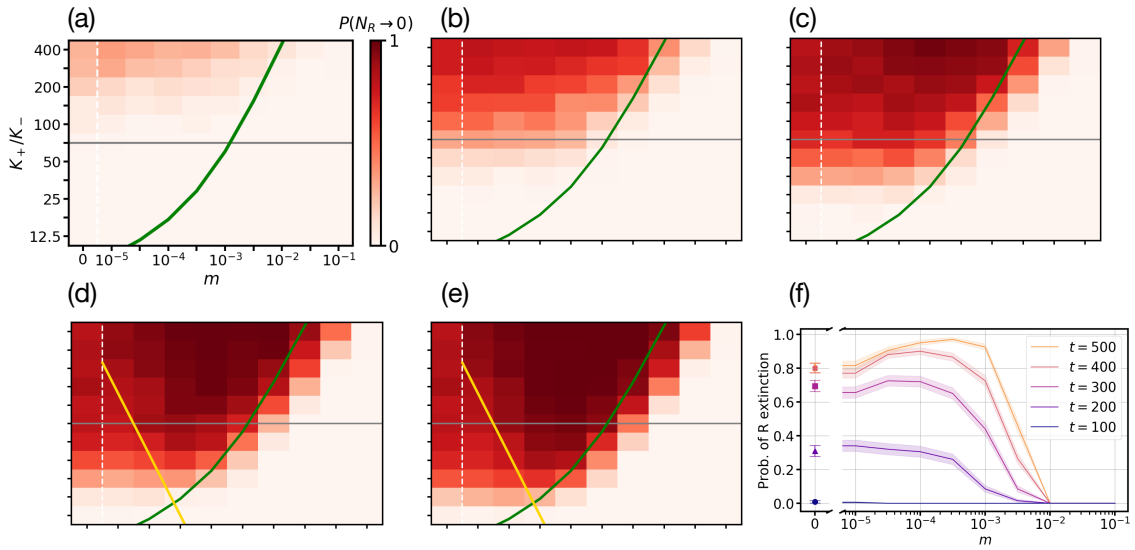

Figure 4: **Slow migration can speed up and enhance the eradication of R cells.** Time evolution of the heatmap showing the probability of R extinction $P(N_R \to 0)$ as a function of bottleneck strength, K_+/K_-, and migration rate m (implemented according to (7)) at **(a)** $t = 100$, **(b)** $t = 200$, **(c)** $t = 300$, **(d)** $t = 400$, and **(e)** $t = 500$ with environmental switching rate $\nu = 0.1$ and bias $\delta = 0.5$; other parameters are as in Table 1 (Methods). As in Fig. 2a, each $(m, K_+/K_-)$ value pair is an ensemble of 200 independent metapopulation simulations and the $P(N_R \to 0)$ colour bar ranges from light to dark red indicating the fraction of simulations that have eradicated R cells at each snapshot in time. The green and dashed white lines represent the theoretical prediction of Eq. (1) and an eye-guiding axis break, respectively (as in Fig. 2a). The golden lines in panels (d-e) show $K_+/K_- = \frac{\nu}{mK_-}$, with $P(N_R \to 0) \approx 1$ in the (upper) region between the golden and green lines, according to Eq. (3) (Discussion). The grey horizontal lines in panels (a-e) indicate the example bottleneck strength of panel (f). **(f)** Probability of R extinction $P(N_R \to 0)$ as a function of migration rate m at bottleneck strength $K_+/K_- = 70.7$. Solid lines (full symbols at $m = 0$) indicate average across 200 realisations; shaded areas (error bars at $m = 0$) indicate binomial confidence interval computed via the Wald interval (Methods).

3 Discussion

Microbial communities live in time-fluctuating environments endowed with spatial structure. Migration in space, environmental variability, and fluctuations thus affect the eco-evolutionary dynamics of bacterial populations [48]. They are particularly relevant to determine the likelihood that cells resistant to antimicrobial drugs survive AMR treatment or thrive in drug-polluted environments [10, 32, 33, 34, 35].

Understanding the joint influence of spatial structure and environmental variability on the evolution of microbial populations is therefore an important research avenue with many open questions. Here, we shed further light on the evolution of cooperative antimicrobial resistance by investigating an *in silico* metapopulation model of sensitive (S) and cooperative resistant (R) cells on a 2D grid of $L \times L$ demes connected through local migration at rate m. The metapopulation is subject to a constant antimicrobial input and time-fluctuating environmental conditions. These are modelled by the carrying capacity K of each deme switching back and forth between a high value ($K = K_+$, mild environment) and a much lower value ($K = K_- \ll K_+$, harsh environment) at a prescribed average rate ν (Fig. 1a). We find that for intermediate switching rate of K, $\nu \lesssim 1$ and for large environmental variability ($K_+/K_- \gg 1$), fluctuations cause the efficient clearance of resistance across the entire metapopulation when migration is slow to moderate, with the migration rate m not exceeding a critical value m_c (for $m < m_c$) that we have estimated analytically in Eq. (1). Slow migration, as is commonly used in microfluidic settings [47], is known to increase fragmentation and influences the evolution of the ensuing sub-populations [16, 49]. We show that, remarkably, slow but non-zero migration can enhance and accelerate the fluctuation-driven eradication of resistant cells ($m = 10^{-4} - 10^{-3}$ in Fig. 4, Fig. 8, and Supplementary Section 3 Movie 2). Our results therefore demonstrate the critical and counterintuitive role of spatial migration that, jointly with environmental variability and demographic fluctuations, determines the maintenance or extinction of cooperative antimicrobial resistance.

Every time the environment suddenly switches from mild to harsh in the intermediate switching regime ($\nu \lesssim 1$), the carrying capacity changes from K_+ to K_- and all demes experience a population bottleneck. When $K_+/K_- \gg 1$, the bottleneck is strong (high environmental variability) and resistant cells are prone to extinction. Demographic fluctuations thus cause R eradication in some demes randomly distributed across the grid (Figs. 1b and 3e,g, Methods, Supplementary Section 3 Movie 3). Critically, resistant cells can migrate and recolonise R-free demes before the next bottleneck occurs, thereby locally reinstating resistance and preventing its global extinction (Figs. 1b and 3b,f,h). When migration is fast enough ($m > m_c$), resistant cells can recolonise more demes than are cleared of R cells by the compounded effects of bottlenecks and demographic fluctuations, and antimicrobial resistance thus survives across the metapopulation. For perfectly isolated demes ($m = 0$), R bacteria cannot recolonise resistant-free demes, and fast resistance extinction is most probable when K_+/K_- is at least of the order of the cooperation threshold N_{th} ($K_+/K_- \gtrsim N_{\text{th}}$) [26] (Fig. 2b-c). Surprisingly, the eradication of resistant cells from the entire metapopulation can be most efficient at slow but non-zero migration, when the R strain is eliminated with a probability close to 1, higher than in the absence of migration (Fig. 4c-f). This stems from R cells having a small chance to take over a deme whenever it experiences the harsh environment (where $K = K_-$) (Methods, Supplementary Section

2). Once this happens, in the absence of migration, resistance survives in any R-only deme (Fig. 8b, Supplementary Section 3 Movie 1). However, when cells migrate at a slow rate m, S can recolonise all demes and the fluctuation-driven eradication mechanism may eliminate all resistance (Methods and Fig. 8, Supplementary Section 3 Movie 2).

The impact of migration on the eradication of R cells is particularly significant when mK_+ (rate of cell migration per deme in the mild environment) is comparable to the frequency at which bottlenecks arise, yielding the condition $mK_+ \gtrsim \nu$ (Methods and Fig. 8c). The probability of eradicating resistant cells in the intermediate switching regime, when $K_+/K_- \gtrsim N_{\text{th}}$, is close to 1 when the migration rate satisfies

$$\nu/K_+ \lesssim m \lesssim m_c \tag{3}$$

(golden and green lines in Fig. 4d-e), corresponding to near-optimal migration rates $m \sim 10^{-4} - 10^{-3}$ in Fig. 4f, which are of the same order as those in typical microfluidic experiments [47]. Remarkably, this demonstrates how migration can be instrumental in eradicating resistance when the environment varies neither too quickly nor too slowly and environmental variability is high. Eventually, after undergoing sufficiently many bottlenecks, the entire red phase in the heatmaps of the probability of R extinction (Figs. 4a-e and 7, Supplementary Fig. 3) becomes fully dark (not shown), corresponding to an R eradication probability 1 for $0 < m \lesssim m_c$ (for $m = 0$ see Discussion and Fig. 8b, Supplementary Section 3 Movie 1). Moreover, we predict that when the population is subject to extreme bottlenecks, $K_+/K_- \gtrsim N_{\text{th}} L^2$ (extreme environmental variability) and $\nu \lesssim 1$, resistance is doomed to go extinct regardless of the migration rate (Methods).

There are different ways of modelling cells' dispersal and migration in microbial populations. Cellular movement is often directed towards areas that are rich in resources [50], but dispersal is commonly assumed to happen with a constant per capita migration rate, e.g., [18, 20]. We are here considering a more general density-dependent form of dispersal (Methods), positing that cells tend to migrate away towards a neighbouring patch when the resident deme occupancy is close to the carrying capacity K (lack of resources), whereas they are less likely to disperse when the local occupancy is well below K (abundance of resources). We have also considered the simpler form of dispersal where all cells can migrate onto a neighbouring deme with a constant per-capita rate m. For both types of migration, we have obtained similar results for the effects of spatial extension and fluctuations on the eradication of resistance (Figs. 5 and 6, Supplementary Section 3 Movies 4-5). These additional data demonstrate that our findings are robust and qualitatively independent of the specific choice of how dispersal is implemented. Extending this work to species-specific or spatially dependent migration rates would be particularly relevant for complex metapopulation structure [15, 20].

In this study, we have specifically focused on a metapopulation model consisting of a 2D grid of

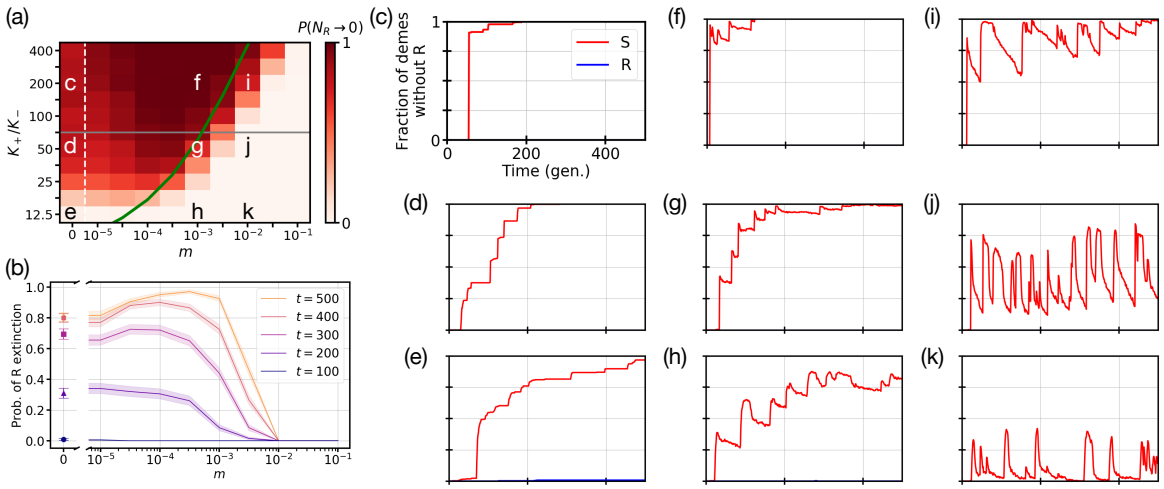

Figure 5: **Revisiting the fluctuation-driven eradication of R cells for intermediate environmental switching with density-dependent migration.** System parameters include an environmental switching rate $\nu = 0.1$, and bias $\delta = 0.5$, with density-dependent migration according to (7). All other parameters $(L, s, a, t_{max}, N_S^0, N_R^0, K_-, N_{\text{th}})$ are as listed in Table 1 (Methods). **(a)** Same heatmap as in Fig. 4e showing the probability of total extinction of R (resistant) microbes, $P(N_R \to 0)$, as a function of bottleneck strength, K_+/K_-, and migration rate m after 500 generations; included as an aid to panels (c-k) for clarity. The color bar in panel (a) varies from light to dark red with the darkest red indicating that eradication of R was found in all 200 realisations, $P(N_R \to 0) = 1$. The white dashed line represents an axis break separating $m = 0$ and $m = 10^{-5}$ on a logarithmic scale. The green line shows the theoretical prediction of Eq. (1). The grey line indicates the bottleneck strength used within panel (b). Annotation letters at specific $(m, K_+/K_-)$ values refer to panels (c-k). **(b)** Same panel as Fig. 4f showing how the probability of R extinction vs migration rate m evolves in time at fixed bottleneck strength, $K_+/K_- = 70.7$. The lines/symbols show the mean across 200 realisations and areas/error bars indicate confidence intervals computed via a Wald interval (Methods). **(c-k)** Temporal evolution of the fraction of R-free demes across the metapopulation for one example realisation in each panel. As indicated in panel (a), migration rates are $m \in \{0, 10^{-3}, 10^{-2}\}$ (left to right) and bottleneck strengths are $K_+/K_- \in \{200, 50, 12.5\}$ (top to bottom). Supplementary Section 3 Movie 4 shows the full spatial metapopulation dynamics for the parameters of panel (i).

$L \times L$ connected by cell migration (Fig. 1b, Methods). This is a natural setting to model microbial communities living on surfaces where cellular migration takes place, with possible applications ranging from the human skin [6], to the digestive tract [7] and plant leaf surfaces [4], the seabed [2], and general wet surfaces [3]. While the results presented here are specific to the above 2D metapopulation model, our main findings on the fluctuation-driven eradication of resistance under slow migration and intermediate switching rate are expected to hold also for other metapopulation structures, such as one-dimensional (1D) cycles or a three-dimensional (3D) lattice of demes. In fact, as long as environmental variability causes population bottlenecks and migration is responsible for the recolonisation of R-free demes, the same behaviour analysed here qualitatively holds independently of the space dimension. However, spatial migration being more limited in 1D than in 2D, we expect that near-optimal clearance of resistance would occur at higher migration rates on a cycle. For the same reasons, we expect that 3D fluctuation-driven resistance clearance should pertain at lower migration rates than in 2D. The impact of other spatial structures (such as star graphs, island models or cliques) has been studied

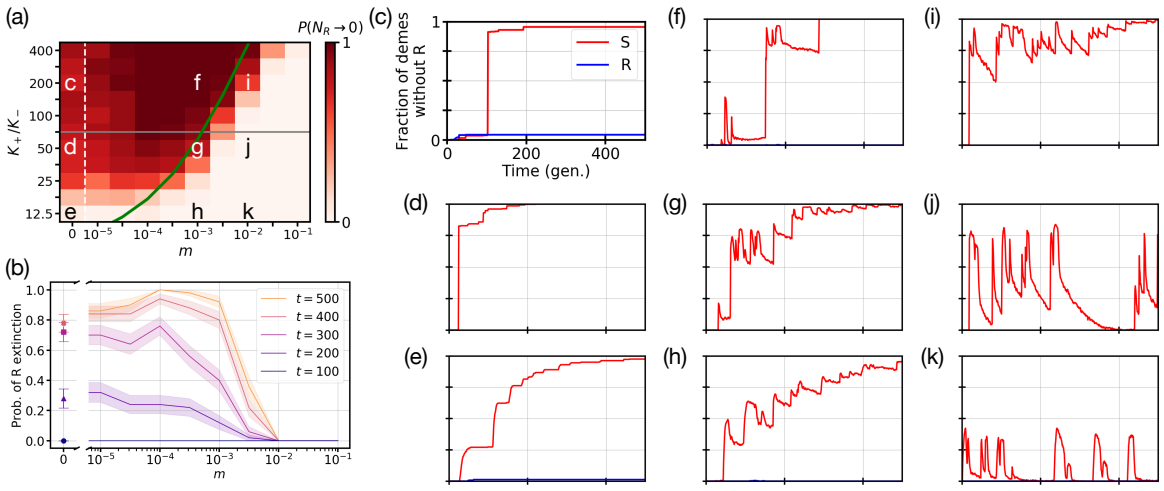

Figure 6: **Exploring the model's robustness: Fluctuation-driven eradication of resistance with density-independent migration.** Same system parameters, $\nu = 0.1$ and $\delta = 0.5$ (see Methods and Table 1 for all parameters), and formatting as in Fig. 5, but the migration rate is here taken density-independent according to (8). **(a)** Fraction of realizations resulting in complete eradication of R cells after 500 microbial generations; the heatmap shows the probability of total extinction of R (resistant) microbes, $P(N_R \to 0)$, depicted by a red colourman varying from light to dark, with the darkest red indicating eradication of R in all 50 realizations ($P(N_R \to 0) = 1$). The same panel elements as in Fig. 5 are shown: a white dashed line representing an axis break for the logarithmic scale, a green line theoretical prediction given by (1), a grey line indicating the bottleneck strength used in panel (b), and letters matching panels (c-k) to their respective $(m, K_+/K_-)$ values. **(b)** Probability of R extinction $P(N_R \to 0)$ as a function of migration rate m for a bottleneck strength of $K_+/K_- = 70.7$ at five different times. The lines/symbols represent the mean across realisations and areas/error bars indicate the confidence intervals computed via the Wald interval (Methods). **(c-k)** Fraction of demes without R cells (red) and without S cells (blue) as a function of time for different values of density-independent migration rate and bottleneck strength: (left to right) $m \in \{0, 10^{-3}, 10^{-2}\}$ and (top to bottom) $K_+/K_- \in \{200, 50, 12.5\}$. Supplementary Section 3 Movie 5 shows the full spatial metapopulation dynamics for the parameters of panel (i).

for non-cooperative resistance, e.g., for constant environments and slow migration [18, 22], and under successive growth-and-dilution cycles coupled to fast cell migration [15, 20]. Understanding the impact of complex spatial structures on cooperative antimicrobial resistance remains mostly an open problem.

Our modelling approach is inspired by chemostat setups. These are commonly used in laboratory-controlled experiments to modulate the influx of nutrients and drugs. The concentration of resources and toxin can thus be set to impose harsh conditions that generate bottlenecks whose impact on the eco-evolutionary dynamics of bacterial populations can be studied [25, 51, 52]. We focus on the biologically relevant regime of intermediate environmental time variation [25, 44, 45], $\nu \lesssim 1$, for which the population size in each deme readily tracks the carrying capacity whereas the local S and R compositions relax more slowly, on a timescale of order $1/s$, with typically $s \sim 10^{-1}$ (Methods, Supplementary Section 1.1). This corresponds to environmental conditions changing from mild ($K = K_+$) to harsh ($K = K_-$) with a frequency once per hour/day, i.e. every 1 to 100 microbial generations (Methods), with the drug influx kept constant and environmental switches occurring rapidly (in < 1 less than one hour). These conditions are all feasible in the laboratory [25, 45], and can in principle

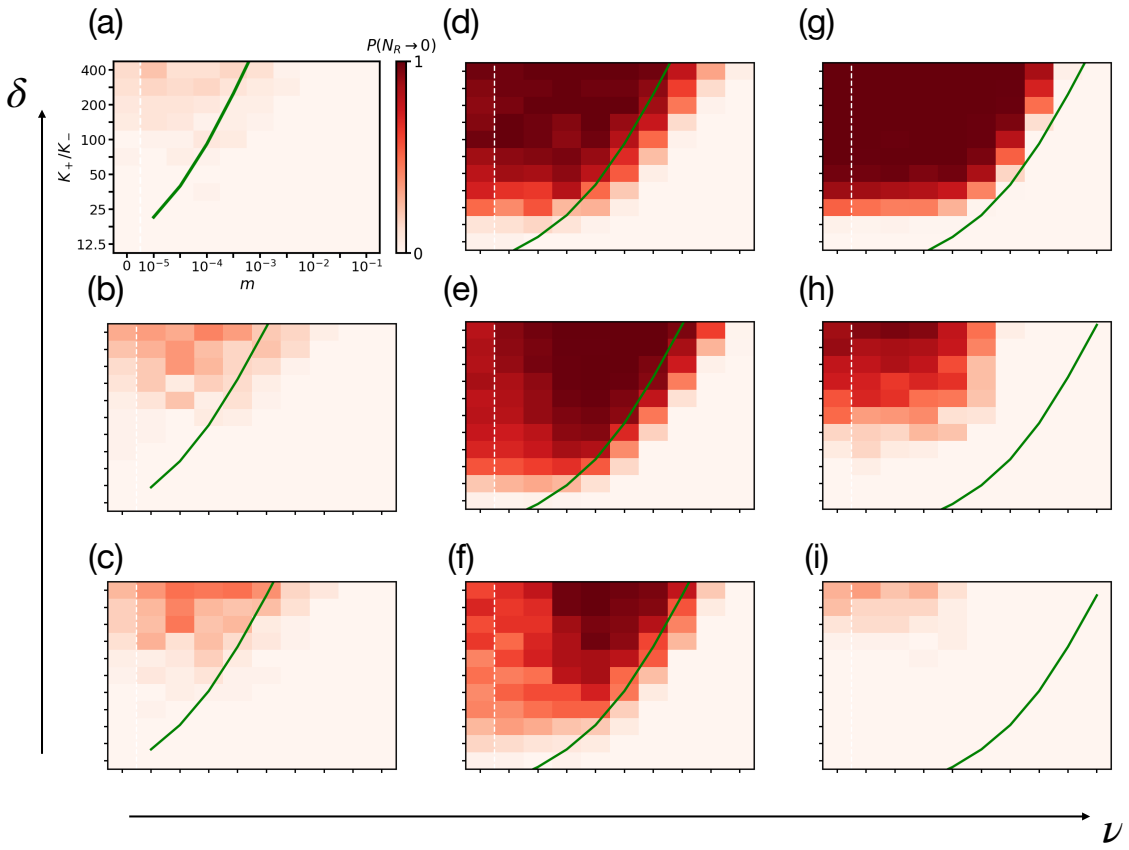

Figure 7: **Exploring the fluctuation-driven eradication of resistance in the (ν, δ) environmental parameter space. (a-i)** Additional heatmaps exploring different environmental switching rates (ν) and biases (δ) showing the probability $P(N_R \to 0)$ of eradicating R cells as a function of the migration rate m (implemented as in (7)) and bottleneck strength K_+/K_- after 500 microbial generations. The colour bar varies from light ($P(N_R \to 0) \approx 0$) to dark red ($P(N_R \to 0) \approx 1$), where the darkest red indicates that all realisations resulted in R eradication across the entire metapopulation, $P(N_R \to 0) = 1$. The white dashed lines and solid green lines indicate axes breaks on the logarithmic scale and theoretical predictions of Eq. (1), respectively. Panels (e) and (g) correspond to Figs. 4e and 2a, with 200 realisations per pixel, whereas each pixel in the other panels results from 50 independent simulations. The environmental switching rate varies from left to right panels, $\nu \in \{0.01, 0.1, 1\}$, and the environmental bias varies from top to bottom, $\delta \in \{0.75, 0.5, 0.25\}$. Additional heat maps can be found in Supplementary Fig. 3.

be realised in a series of spatially connected chemostats, each acting as a deme, with the rate of cell migration set by the partial mixing between neighbouring demes-chemostats with fixed volumes. While we have conveniently represented the switching of the carrying capacity as random processes occurring at rates $\nu_\pm$ (Fig. 1a), an essentially equivalent practical implementation would let K vary periodically between K_+ and K_- with a period $1/\nu_+ + 1/\nu_-$ [39] (Methods, Supplementary Section 1.2).

We have carried out extensive stochastic simulations of the ensuing metapopulation dynamics, and repeatedly tracked the evolution of up to 10^7 microbes distributed across 400 spatial demes through hundreds of realisations, and thousands of different environmental parameters and migration rates (Methods). While this is a rather large metapopulation model, most experiments are carried out with bigger microbial populations [33, 53, 54]. We nevertheless expect that spatial fluctuation-driven

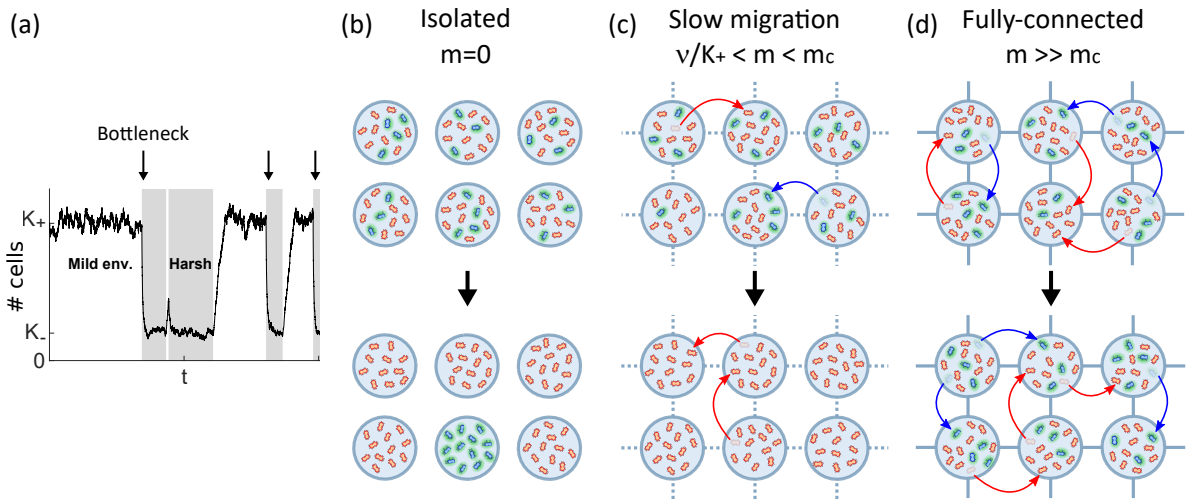

Figure 8: **How slow migration enhances the eradication of resistant cells. (a)** Example evolution of the total number of cells in a deme ($N = N_S + N_R$), driven by the fluctuating carrying capacity $K(t)$, in an environment switching at intermediate rates $\nu_\pm \lesssim 1$. As the environment continuously alternates between mild and harsh conditions, the carrying capacity varies suddenly from $K = K_+$ (mild, white background) to $K = K_- \ll 1$ (harsh, grey background), bottlenecks appear (arrows), and the fluctuation-driven eradication of R cells (Figs. 1a bottom and 3a, Methods) sets in. Here, parameters are $\nu_- = 0.125$, $\nu_+ = 0.075$, $K_- = 80$, $K_+ = 400$. Panels **(b)-(d)** schematically illustrate the state of the metapopulation before (top row) and after (bottom) several consecutive bottlenecks at intermediate switching for three migration scenarios. **(b)** The metapopulation initially consists of demes containing both R and S cells (top, blue and red cells). After several environmental bottlenecks (black downward arrow, N dynamics as panel (a)), the fluctuation-driven eradication mechanism can clear resistance from most demes (Methods). However, when $m = 0$ (no migration), R cells may randomly take over a few demes (bottom, blue-only, Supplementary Section 3 Movie 1) and survive locally. (Following bottlenecks, R and S could still coexist in some demes, and more bottlenecks would be needed to eradicate R, not shown here). **(c)** Same as in panel (b) with demes connected by slow migration of cells (red/blue curved arrows indicating S/R migrations, $\nu/K_+ < m < m_c$; Discussion and Methods). In this scenario, even if R cells take over a few demes, S cells can migrate and recolonise these demes (Supplementary Section 3 Movie 2), which then become prone to the fluctuation-driven resistance extinction (bottom, all red, $m = 10^{-4} - 10^{-3}$ in Fig. 4, Methods). **(d)** Same as in (b)-(c) when cells migrate at a high rate ($m \gg m_c$, Eq. (2), Methods), where the metapopulation effectively consists of fully-connected demes. In this scenario, many migration events occur (red and blue arrows), which continuously mix up the composition of the demes, preventing the fluctuation-driven eradication to clear resistance; R and S cells typically coexist in all demes.

eradication occurs also in large and more extended bacterial populations provided the conditions (2), which can be met in typical microbial communities (Methods), are actually satisfied. Moreover, with microfluidic devices and single-cell techniques, it is possible to perform spatially structured experiments with only 10 to 100 cells per 'microhabitat patch' [9, 47, 55], which are conditions compatible with our modelling parameters ($K_- = 80$).

It is worth noting that most laboratory experiments are carried out with batch cultures (growth-dilution cycles), e.g. [15, 56], which are easier to run than chemostat or microfluidic setups. However, the concentration of nutrients (microbial consumption) and drug (enzymatic degradation by R cells) changes continuously in batch culture experiments, rendering their explicit modelling challenging [20, 57]. The 2D metapopulation considered here, when short periods in the harsh environment ($K = K_-$) are followed by extended sojourns in the mild environment ($K = K_+$), while the drug concentration would be assumed to remain roughly constant, may be viewed as approximately mimicking the growth-

dilution cycles of batch cultures. The dynamic degradation of the drug can however play a critical role in the evolution of cooperative AMR, as shown in Ref. [21], where the fragmentation of the metapopulation into isolated demes enhances the maintenance of resistance.

While we have here focused on a two-strain metapopulation model, our main results can be extended to the eradication of resistant (R) cells from microbial populations consisting of multiple sensitive strains continuously experiencing mild and harsh environmental conditions in turn. To this end, the fraction of R cells in each deme should fluctuate about a low, non-zero value (here, $N_{\rm th}/K_+ \ll 1$, Fig. 1). Additionally, the spatial fluctuation-driven eradication of resistance requires that the number of cells in each deme decreases sharply following a population bottleneck, while the deme composition evolves on a slower timescale, yielding a small R subpopulation prone to extinction in each deme. In our model, there are approximately $N_{\rm th}K_-/K_+ \lesssim 1$ resistant cells in each deme after a bottleneck has occurred (Fig. 1, Methods). In the case of non-cooperative antimicrobial resistance, the fraction of resistant cells does not fluctuate about a small non-zero value, and the spread of sensitive bacteria is always hampered by the drug (Methods). Hence, in non-cooperative resistance, if there are initially sufficiently many R cells, resistance can take over the whole metapopulation [18, 20].

Environmental variations, spatial structure, cellular migration, and fluctuations are all ubiquitous key factors influencing the evolution of cooperative antimicrobial resistance. The joint effect of dispersal and fluctuations is particularly complex and poses a number of challenges [46, 48, 58]. In this study, we have demonstrated by theoretical and computational means that environmental variability and migration can lead to the efficient eradication of drug resistance from a 2D metapopulation. We have determined the origin and the near-optimal conditions for fluctuation-driven eradication of resistance in a spatial setting. To achieve this goal, the environment needs to change at an intermediate switching rate ($\nu \lesssim 1$), and environmental variability has to be strong enough ($K_+/K_- \gtrsim N_{\rm th}$, assuming $N_{\rm th} < K_- < K_+$) to generate a succession of population bottlenecks in each metapopulation deme where the local resistant population can be driven to extinction by demographic fluctuations. Resistant cells' migration can recolonise demes free of R cells, and hence often help maintain resistance. However, we have shown that strong bottlenecks may limit and effectively counter the recolonisation by dispersal. This results in a trade-off arising at $\nu/K_+ \lesssim m \lesssim m_c$, when slow but nonzero migration and sufficiently strong bottlenecks can act most synergistically to eradicate resistance by accelerating and enhancing the spatial fluctuation-driven eradication mechanism. We argue that these conclusions hold for microbial populations of realistic size and can be extended to other spatial structures. Our findings are robust against different forms of migration and are expected to hold for multi-strain communities. We have also discussed their relevance to batch cultures and propose feasible laboratory experiments [25, 51, 52]. We believe that our work can inform novel treatment protocols and pave

the way to explore innovative alternative treatment options to prevent the spread of antimicrobial resistance in clinical and other applications.

Parameter	Description	Value
L	side length of square lattice	20
t_{max}	maximum number of microbial generations	500
N_{S}^0	average number of S cells per deme at $t = 0$	$K(t = 0) - N_{\mathrm{th}}$
N_{R}^0	average number of R cells per deme at $t = 0$	N_{th}
a	reduction in the birth rate of S cells due to drug exposure	0.25
s	resistance metabolic cost for R cells	0.1
m	migration rate	0–10^{-1}
K_+	carrying capacity per deme in the mild environment	10^3–$3.2 \cdot 10^4$
K_-	carrying capacity per deme in the harsh environment	80
N_{th}	cooperation threshold	40
ν	environmental switching rate	10^{-2}–10^0
δ	environmental switching bias	0.25–0.75

Table 1: **Summary of simulation parameters.** Parameters kept fixed are listed by a single value, other parameters are listed as ranges. The average number of sensitive cells S per deme at $t = 0$ (N_S^0) equals the metapopulation's carrying capacity at $t = 0$ minus the constant threshold value for cooperation, $K - N_{\mathrm{th}}$, which depends on whether the system begins in a harsh or mild environment, $K \in \{K_+, K_-\}$. See Supplementary Fig. 3 for an extended range in ν and δ.

4 Methods & Model

4.1 Microbial model for an isolated deme

A common mechanism of antimicrobial resistance is based on *drug exposure protection*. Usually, it involves resistant cells investing metabolic resources to produce enzymes that hydrolyse antimicrobial drugs [42, 59, 60]. An example is the inactivation of the broad class of β-lactam antibiotics by the β-lactamase enzyme [43] that is often produced by resistant cells carrying gene-bearing plasmids commonly used in laboratory experiments [42, 61]. This resistance mechanism can lead to a form of AMR cooperative behaviour when drug-sensitive cells are protected from the toxin without paying any metabolic cost. Inspired by β-lactamase AMR, we here assume that each R cell produces the resistance enzyme at a fixed rate. The associated extra metabolic cost reduces the R growth rate and hence lowers the resistant cells' fitness f_R from its baseline value set to 1. Assuming that resistance entails a constant fitness cost $s > 0$, the R fitness is set as $f_R = 1 - s > 0$ regardless of the local drug concentration. When sensitive bacteria are not exposed to the toxin, they grow faster than R cells and have a baseline fitness $f_S = 1$ higher than f_R (no extra metabolic cost for S). However, the spread of S cells is hindered when they are in contact with the drug, and their fitness is then reduced to $f_S = 1 - a < f_R$. Sensitive bacteria recover the baseline fitness $f_S = 1$ when the number of R microbes N_R reaches the *cooperation threshold* N_{th}. When $N_R \geq N_{\mathrm{th}}$, the resistance enzyme concentration in a

deme is sufficiently high to locally protect all microbes from the toxin [26, 28, 42, 59, 60] (Fig. 1a). This scenario models the effect of biostatic antimicrobial drugs at low concentration in demes/chemostats whose volume is kept constant, a regime in which the action of biocidal and biostatic toxins is similar [62, 63]. The per-capita death rate of any cell in a deme is N/K, where $N = N_R + N_S$ is the population size in the deme and K denotes the same carrying capacity of each deme. The composition of each deme evolves stochastically according to the microbial birth and death reactions

$$\begin{aligned} N_{R/S} &\longrightarrow N_{R/S} + 1 \quad \text{with rate } \frac{f_{R/S}}{\bar{f}} N_{R/S}, \\ N_{R/S} &\longrightarrow N_{R/S} - 1 \quad \text{with rate } \frac{N}{K} N_{R/S}. \end{aligned} \tag{4}$$

Here, the R/S birth rate in a deme is given by the fitness $f_{R/S}$ relative to the average fitness in the deme $\bar{f} = (f_R N_R + f_S N_S)/N$ [26, 27, 28, 37, 38, 39]. The choice $f_{R/S}/\bar{f}$ for the birth rate allows us to establish a relationship with the well-known Moran process, a reference model in mathematical biology [26, 37, 38, 64, 65]. The master equation of this multivariate continuous-time birth-death process is given in the supplementary information (Supplementary Section 1.3). The resulting eco-evolutionary dynamics is characterised by a fast dynamics of the total number of microbes in each deme, N, that is driven by the fluctuating carrying capacity K and reaches a quasi-stationary distribution after very few microbial generations, i.e. on a ecological timescale ~ 1 (Supplementary Fig. 1 and Supplementary Section 1.2). Since $s \lesssim 1$, the fraction of R and S cells composing a deme evolves on a slower evolutionary timescale $\sim 1/s$ (at rate $f_S - f_R \sim s$). We note that the intermediate environmental switching regime mentioned previously, see, e.g., Eq. (2), refers to an average switching rate $\nu \sim s \lesssim 1$. In a static environment, the number of R cells fluctuates about the cooperation threshold $N_R \approx N_{\text{th}}$, while there are $N_S \approx K - N_{\text{th}}$ sensitive cells (Fig. 1a; Supplementary Fig. 2 and Supplementary Section 2). In our examples, we have chosen a realistic small value $s = 0.1$ for the extra metabolic cost associated with resistance, and a plausible reduction of 25% of f_S, with $a = 0.25$, when S cells are exposed unprotected to the drug [63, 66, 67]. These values are indicative, but we expect that the results reported here should qualitatively hold for a broad range of parameters [26].

4.2 Environmental dynamics

Environmental variability, random or periodic, refers to changes in external conditions that are ubiquitous and commonly arise at the microscale. Variations of the environment shape microbial populations by coupling their ecological and evolutionary dynamics (eco-evolutionary dynamics) [23], e.g., the changes in the size and composition of a population in a deme are dynamically interdependent [24, 68]. The amplitude of demographic fluctuations is modulated by environmental variability, and this cou-

pling is particularly important in small populations [23, 24, 37, 38, 39, 40, 41, 69]. Here we wish to model continuous sudden and drastic environmental changes, like the occurrence of regular population bottlenecks. To this end, we assume that a random telegraph process $\xi(t) \in \{-1, 1\}$ drives the carrying capacity $K(t)$ of each deme. The coloured dichotomous Markov noise ξ switches back and forth according to $\xi \longrightarrow -\xi$ at rate $\nu_\pm$ when $\xi = \pm 1$ [70, 71]. Environmental variability is thus modelled by writing the *time-dependent* carrying capacity as [26, 27, 28, 37, 38, 39, 40, 41, 69]

$$K(t) = \frac{1}{2}\left[K_+ + K_- + \xi(t)\left(K_+ - K_-\right)\right], \tag{5}$$

with K switching back an forth from K_+ when the environment is mild ($\xi = 1$) to $K_- < K_+$ in a harsh environment ($\xi = -1$) at rate $\nu_\pm$ [26, 27, 28, 37, 38, 39, 40, 41, 69, 70, 71, 72] (Fig. 1a), according to

$$K_+ \underset{\nu_-}{\overset{\nu_+}{\rightleftharpoons}} K_-. \tag{6}$$

For our analysis, it is convenient to introduce the mean switching rate $\nu = (\nu_- + \nu_+)/2$, and the switching bias $\delta = (\nu_- - \nu_+)/(\nu_- + \nu_+)$, where $|\delta| \leq 1$, and $\delta > 0$ when more time is spent on average in the mild environment. The stationary population distribution in each deme can be approximated analytically by focusing on the fluctuating carrying capacity (5). It is bimodal with peaks at K_+ and K_- ($N \approx K_\pm$) when the environment varies very slowly, $\nu \ll 1$. When $\nu \gg 1$, the environment varies very quickly and N is unimodally distributed around its peak at $N \approx 2K_+K_-/[(1-\delta)K_+ + (1+\delta)K_-]$ [26, 39] (Supplementary Fig. 2 and Supplementary Section 1.2). When $\nu \sim s$, the population size in each deme tracks the carrying capacity, and a population bottleneck arises each time the carrying capacity switches from K_+ to K_-, which occurs at an average frequency $\nu_+\nu_-/(2\nu) = \nu(1-\delta^2)/2$. Modelling environmental changes using the telegraph process is a natural and simple choice. We note that dichotomous noise is simple to simulate, amenable to mathematical analysis (Supplementary Section 1.2), and it can naturally describe the binary fluctuating environmental conditions that are commonly used in laboratory-controlled experiments [25, 45, 51, 52]. While more complex forms of noise can be considered, the choice made here is therefore biologically relevant and convenient (Supplementary Section 1.2).

4.3 Spatial structure and cell migration

Microbial populations generally evolve in spatially structured environments in which cells can migrate [73, 74]. Spatial migration can be coupled to ecological changes and evolutionary dynamics [15, 21, 22], and is generally thought to moderate local fluctuations, with higher migration between sites homogenizing the local population composition [58]. Here, we study a metapopulation embedded

in a 2D spatial grid of $L \times L$ demes (with periodic boundary conditions) modelling a surface-attached microbial population [2, 3, 4, 6, 7] (Fig. 1b). These are connected by cell migration between neighbouring sites. In our study, we have considered two forms of migration: (i) We have assumed that all cells in a deme $\vec{u}$ have a density-dependent per-capita migration rate $mN(\vec{u})/K(t)$, which increases as the deme's population size $N(\vec{u})$ approaches the carrying capacity, i.e., when available resources are subject to local constraints. (ii) We have also considered the simpler form of migration where all cells in a deme $\vec{u}$ feature the same constant per capita migration rate m (Fig. 6 and Supplementary Section 3 Movie 5). We represent these two forms of migration by picking randomly a cell (either R or S) from deme $\vec{u}$ and moving it into a nearest-neighbour $\vec{u}'$ according to the following stochastic reactions:

$$\text{(i)} \quad \left(N\left(\vec{u}\right), N\left(\vec{u}'\right)\right) \longrightarrow \left(N\left(\vec{u}\right)-1, N\left(\vec{u}'\right)+1\right), \text{ with rate } \frac{m}{4}\frac{N(\vec{u})}{K(t)}N(\vec{u}). \tag{7}$$

$$\text{(ii)} \quad \left(N\left(\vec{u}\right), N\left(\vec{u}'\right)\right) \longrightarrow \left(N\left(\vec{u}\right)-1, N\left(\vec{u}'\right)+1\right), \text{ with rate } \frac{m}{4}N(\vec{u}), \tag{8}$$

where the destination deme $\vec{u}'$ is randomly picked between the four nearest neighbours of $\vec{u}$. The results reported in Figs. 2, 3, and 4 were obtained with the density-dependent form of migration (7). However, we have confirmed that the specific form of migration does not qualitatively affect our findings for the fluctuation-driven eradication of resistance at intermediate environmental switching rates, as demonstrated by the comparison of Figs. 5 and 6 (Discussion, Supplementary Section 3 Movies 4-5).

Since most migrations occur when the population resides in the mild environmental state where $K = K_+$ and the number of microbes in each deme is typically large, we can estimate the rate of migration per deme in the intermediate switching regime (where $\nu \sim s$) as mK_+. The impact of migration on microbial dynamics is most striking when there is at least one cell migrating into each deme between consecutive bottlenecks. Matching the rates at which these events occur yields $m \gtrsim \nu/K_+$. Migration rates lower than ν/K_+ (i.e. $m < 10^{-3.5}$ in Fig. 2 and $m < 10^{-4.5}$ in Fig. 4) lead to the same probability of R eradication as $m = 0$, whereas migration efficiently rescues resistance when $m > m_c$, see Eq. (1). The master equation of the full metapopulation model with migration and switching carrying capacity in each deme is given in Supplementary Section 1.3.

4.4 Fluctuation-driven eradication mechanism with spatial migration

Fluctuation-driven eradication of resistance in a deme arises when the carrying capacity switches between K_+ and K_- at rate $\nu \sim s$, generating strong enough population bottlenecks ($K_+/K_- \gtrsim N_{\text{th}}$). In this regime, the number of microbes in the deme continuously tracks the carrying capacity, while the deme's composition evolves on a slower timescale $\sim 1/s$. After each bottleneck, the fraction of R cells in the deme initially fluctuates about $N_{\text{th}}/K_+ \ll 1$, and their expected number in the harsh

environment, $N_R \approx N_{\rm th}K_-/K_+ \lesssim 1$, is sufficiently low for demographic fluctuations to effect the eradication of resistance [26].

Hence, we assume that approximately K_- cells are randomly drawn to survive a bottleneck. Given that the number of cells before the bottleneck is sufficiently high ($K_+ \gg 1$), each R cell survives with the same independent probability (random draws with replacement), which matches the fraction of R cells, that is approximately $N_{\rm th}/K_+$. Therefore, the number of R cells surviving one bottleneck can be drawn from a Poisson distribution of mean $N_{\rm th}K_-/K_+$, and the probability that one bottleneck eradicates resistance yields $\exp\left(-\frac{N_{\rm th}K_-}{K_+}\right)$. In this regime, the fluctuation-driven clearance of AMR is attempted at each bottleneck (Fig. 1a). AMR fluctuation-driven eradication thus occurs at a rate comparable to the bottleneck frequency, given by $\frac{\nu_-\nu_+}{2\nu} = \nu\left(1-\delta^2\right)/2$. Consequently, the rate at which each deme becomes R-free is approximately $\frac{\nu_-\nu_+}{2\nu}\exp\left(-\frac{N_{\rm th}K_-}{K_+}\right)$.

The demes of the metapopulation are connected by cell migration, which generally homogenizes the local population composition [58] and here tends to favour the coexistence of R and S cells [46]. Noting that the fraction of demes where resistance survives a single bottleneck can be approximated by $1-\exp\left(-\frac{N_{\rm th}K_-}{K_+}\right)$, we can estimate that the total rate of resistant cells migrating from each of these demes is $mN_{\rm th}\left[1-\exp\left(-\frac{N_{\rm th}K_-}{K_+}\right)\right]$. Matching this rate of migration of R cells with the rate at which a deme becomes R-free, $\frac{\nu_-\nu_+}{2\nu}\exp\left(-\frac{N_{\rm th}K_-}{K_+}\right)$, we obtain the critical migration rate m_c.

When $m \gg m_c$, see Eq. (1), numerous cells migrate between successive bottlenecks. This efficiently mixes up the local population composition, and helps maintain resistance by recolonising R-free demes (Figs. 1b and 8d). However, when $\nu/K_+ \lesssim m \lesssim m_c$, the rate of cell migration per deme is comparable to the bottleneck frequency, and migration thus enhances and speeds up the eradication of resistance (Discussion, Fig. 4). When $\nu/K_+ \lesssim m \lesssim m_c$ and $\nu \sim s$, sensitive cells can recolonise any R-only deme, and resistant cells are prone to be driven to extinction by fluctuations (Figs. 1b and 8c). For this spatial fluctuation-driven eradication mechanism to work efficiently, the rate of environmental variability should neither be too low, ensuring that recolonisation does not reinstate resistance, nor too high in order to guarantee the production of bottlenecks, and more time be spent in the mild environment (on average) for coexisting demes to consist overwhelmingly of S cells when bottlenecks occur. We have thus found that the frequencies in the range $s/10 \leq \nu \leq 10s$ and a switching bias $\delta \geq 0$ ($0.01 \leq \nu \leq 1$, $0 \leq \delta \leq 0.90$ in Fig. 7 and Supplementary Fig. 3) optimise the spatial fluctuation-driven eradication of resistance. Slow migration is most effective in speeding up and enhancing the fluctuation-driven clearance of R cells when $\nu \sim s$ and $\delta > 0$ (Fig. 7; Supplementary Fig. 3; and Supplementary Section 3, Movies 1-3). In the limit of very fast migration, $m \gg 1$, the metapopulation can be regarded as L^2 fully connected demes (island model [75, 76]), all subject to the same fluctuating carrying capacity $K(t)$. In this case, the fraction of R cells just after an environmental bottleneck still

fluctuates about $N_{\rm th}/K_+$ in each of the fully connected sites, all experiencing the carrying capacity K_-. The approximate total number of R cells across the metapopulation right after a bottleneck is thus $L^2 N_{\rm th} K_-/K_+$. When $m \gg 1$, resistance can typically be eradicated if all R cells are eliminated simultaneously during a single bottleneck. This can occur when the expected total number of R cells after a bottleneck is of order 1, i.e., for very strong bottlenecks $K_+/K_- \gtrsim N_{\rm th} L^2$. Hence, when $\nu \sim s$ and $m \gg 1$, fluctuation-driven eradication of resistance occurs for very strong bottlenecks, $K_+/K_- \gtrsim N_{\rm th} L^2$, independent of the actual value of m.

Finally, we expect that the above fluctuation-driven eradication of AMR in spatially structured environments holds when conditions (2) are satisfied by the typically big microbial populations found in nature [33, 53, 54], e.g., $(K_+, K_-, N_{\rm th}) \sim (10^{11}, 10^6, 10^5)$.

4.5 Computational methods

In this section, we explain how the extensive stochastic simulations of the metapopulation dynamics were performed and summarise the parameters that we have used.

4.5.1 Metapopulation simulations

A natural extension to the non-spatial model of a well-mixed microbial community is through agent-based lattice simulations. This work employs a stochastic Monte Carlo algorithm on a two-dimensional, $L \times L$, square lattice (metapopulation) with periodic boundary conditions to investigate interaction effects of diffusively-coupled neighbouring microbial communities. The Gillespie algorithm [77] was also considered, but due to the amount of cells within each deme and overall size of the metapopulation, it was deemed less computationally efficient. Each microbial community (deme) within the lattice contains sensitive and resistant cells whose populations are governed by a birth-death process with migration and are subject to a fluctuating carrying capacity, according to (4)-(8). To minimize initial transients, at $t = 0$ a total of $N_{\rm th} L^2$ resistant and $(K - N_{\rm th})L^2$ sensitive cells (with $K \in \{K_-, K_+\}$) are uniformly distributed at random among all L^2 demes in the metapopulation. The expected initial number of resistant and sensitive cells here matches their respective stationary population in a static environment, $N_R^0 = N_{\rm th}$ and $N_S^0 = K - N_{\rm th}$ (Methods). Further, the environmental state of the metapopulation at $t = 0$ begins at stationarity, $K(t = 0) = \langle K(t) \rangle = \frac{1}{2}\left[K_+ + K_- + \delta(K_+ - K_-)\right]$ with the mean of the dichotomous Markov noise equalling that of the environmental switching bias, $\langle \xi(t) \rangle = \delta$ [26, 39]. Thus, the system begins in a harsh (K_-) or mild (K_+) environment with a probability of $(1 - \delta)/2$ or $(1 + \delta)/2$, respectively. We ran 200 realisations for each parameter set of Figs. 2, 4, 5, and 7e,g, and ran 50 realisations for each parameter set in Fig. 6 and all panels of Fig. 7 (except for panels e and g). Each panel of Fig. 3 features the same single simulation realisation.

Results reported in Figs. 1a (bottom) and 8a for the dynamics in a single isolated deme were obtained using the classical Gillespie algorithm [77].

The system evolves in time units of microbial generations, where we consider one generation to equal one Monte Carlo Step (MCS), e.g., bacteria replicate on a scale of roughly once every ~ 1 hour. Within every generation, the environment can switch at rate ν and cells are chosen at random to attempt birth, death, or migration reactions as described by Eqs. (4), (7), and (8). We have used two forms of migration: one where the per capita migration rate depends on the deme's local population density, Eq. (7), and a simpler case where that rate is constant, Eq. (8). Migration has been implemented in the same way for both formulations. A single MCS is said to be completed once the number of death or birth reactions equals twice the current number of cells within the system, 1 MCS $= 2\sum_{\vec{u}}(N_{\mathrm{S}}(\vec{u}) + N_{\mathrm{R}}(\vec{u}))$ where the sum is over all the demes, $\vec{u}$. There are thus $\sim 10^4$ birth/death events in 1 MCS when $N(\vec{u}) = N_S(\vec{u}) + N_R(\vec{u}) \approx K_-$ in each deme $\vec{u}$, and $\sim 10^5 - 10^7$ events when $N(\vec{u}) \approx K_+$. Therefore, on average, each cell in the system attempts one birth and one death reaction within a generation. Since the simulation time unit is set as one microbial generation, migration reactions and environmental switches do not contribute to the above reaction count. This allows for a direct comparison between simulations at different migration m and environmental rates ν. For all finite stochastic systems with an absorbing state, the final equilibrium corresponds to the absorption in that state. In our model, the ultimate absorbing state is characterised by the total extinction of both microbial strains. However, this is unobservable in a reasonable amount of computational time (or in real microbial communities) as this phenomenon occurs on a timescale that diverges dramatically with the total population and the size of the grid of demes. In our study, we ran simulations for up to 500 generations, which is of the order of 10^2 experimental hours. This is sufficiently long to observe the fluctuation-driven eradication of R cells in the metapopulation (when feasible), but short enough to maintain computational efficiency.

4.5.2 Simulation parameters

To run a single simulation, 12 parameters are specified: the side length of the square lattice of demes, L; the duration of the simulation (number of microbial generations), $t_{\max}$; the average initial number of sensitive and resistant cells per deme at $t = 0$, N_S^0 and N_R^0; the impact of the drug on the fitness of exposed sensitive cells, a; the constant metabolic cost for resistant cells to generate the resistance enzyme, s; the migration rate, m; the mild and harsh carrying capacity in each deme, K_+ and K_-; the resistant cooperation threshold, N_{th}; the average environmental switching rate, ν; and the environmental bias, δ. Throughout this work, we fixed seven parameters in all lattice simulations for computational convenience: $L = 20$, $t_{\max} = 500$, $N_R^0 = 40 = N_{\mathrm{th}}$, $a = 0.25$, $s = 0.1$, and $K_- = 80$.

The remaining parameters are specified within the figure captions. All parameters are summarised in Table 1. In our figures, we have explored and characterised the spatial fluctuation-driven eradication of R across the two-dimensional metapopulation by tuning the average switching rate ν, the environmental switching bias δ determining the relative time spent in mild/harsh conditions, the migration rate m, and the bottleneck strength K_+/K_- (keeping K_- fixed).

The explored range of migration rates varies from small to large migration values, $m \in [10^{-5}, 10^{-1}]$, as well as the case of absent migration, $m = 0$ (separated by vertical dashed white lines in Figs. 2, 4, and 7, and Supplementary Fig. 3). We simulated a range of values of the demes' carrying capacity K_+ in the mild environment, with K_+ spanning from 10^3 to $3.2 \cdot 10^4$. The environmental bottleneck strength K_+/K_- thus ranged from 12.5 to 400. The upper limit in K_+ and the side length of the square grid L set the maximum total number of cells across the grid of demes ($\sim L^2 K_+$), which was bounded by $\sim 10^7$ due to computational constraints (Discussion). We also tested an extended range of intermediate environmental switching parameters to corroborate our results, with $\nu \in \{0.01, 0.1, 1\}$ and $\delta \in \{0.25, 0.5, 0.75\}$ (Fig. 7; see Supplementary Fig. 3 for additional slow and fast switching environments).

5 Data availability

The data generated and used within this work can be found at the Open Science Framework repository (Lluís Hernández-Navarro, Kenneth Distefano, Uwe C. Täuber, and Mauro Mobilia. 2024. Supplementary data, code, and videos for "Slow spatial migration can help eradicate cooperative antimicrobial resistance in time-varying environments". OSF. https://doi.org/10.17605/OSF.IO/EPB28).

6 Code availability

The C++ code used to generate the data and the Python and Matlab codes to process and visualize the data within this work can be found at the Open Science Framework repository (Lluís Hernández-Navarro, Kenneth Distefano, Uwe C. Täuber, and Mauro Mobilia. 2024. Supplementary data, code, and videos for "Slow spatial migration can help eradicate cooperative antimicrobial resistance in time-varying environments". OSF. https://doi.org/10.17605/OSF.IO/EPB28).

Acknowledgements

The authors would like to thank M. Asker, J. Jiménez, S. Muñoz Montero, M. Pleimling, A. M. Rucklidge, and M. Swailem for fruitful discussions. L. H. N. and M. M. gratefully acknowledge funding

from the U.K. Engineering and Physical Sciences Research Council (EPSRC) under the Grant No. EP/V014439/1 for the project 'DMS-EPSRC Eco-Evolutionary Dynamics of Fluctuating Populations' (https://eedfp.com/). K. D. and U. C. T.'s contribution to this research was supported by the U.S. National Science Foundation, Division of Mathematical Sciences under Award No. NSF DMS-2128587.

Author information

These authors contributed equally: Lluís Hernández-Navarro & Kenneth Distefano.

Department of Applied Mathematics, School of Mathematics, University of Leeds, Leeds LS2 9JT, U.K.

Lluís Hernández-Navarro & Mauro Mobilia.

Department of Physics & Center for Soft Matter and Biological Physics, MC 0435, Robeson Hall, 850 West Campus Drive, Virginia Tech, Blacksburg, VA 24061, USA

Kenneth Distefano & Uwe C. Täuber.

Faculty of Health Sciences, Virginia Tech, Blacksburg, VA 24061, USA

Uwe C. Täuber.

Author contributions

Conceptualization: Lluís Hernández-Navarro, Mauro Mobilia.

Data curation: Kenneth Distefano, Lluís Hernández-Navarro.

Formal analysis: Lluís Hernández-Navarro, Kenneth Distefano, Mauro Mobilia.

Funding acquisition: Mauro Mobilia, Uwe C. Täuber.

Investigation: Lluís Hernández-Navarro, Kenneth Distefano.

Methodology: Lluís Hernández-Navarro, Kenneth Distefano, Mauro Mobilia.

Project administration: Mauro Mobilia.

Resources: Uwe C. Täuber, Mauro Mobilia.

Software: Kenneth Distefano.

Supervision: Mauro Mobilia, Uwe C. Täuber.

Validation: Kenneth Distefano, Lluís Hernández-Navarro.

Visualization: Lluís Hernández-Navarro, Kenneth Distefano, Mauro Mobilia.

Writing – original draft: Lluís Hernández-Navarro, Mauro Mobilia, Kenneth Distefano.

Writing – review & editing: Lluís Hernández-Navarro, Mauro Mobilia, Kenneth Distefano, Uwe C. Täuber.

Corresponding authors

Correspondence and requests for materials should be addressed to Lluís Hernández-Navarro or Mauro Mobilia.

Ethics declarations

Competing interests

The authors declare no competing interests.

Supplementary Information

Supplementary Information can be found at the *bioRxiv* repository:
https://www.biorxiv.org/content/10.1101/2024.12.30.630406v1.supplementary-material.

References

[1] Bickel S, Or D. Soil bacterial diversity mediated by microscale aqueous-phase processes across biomes. Nat Commun. 2020;11(1):116.

[2] Dann LM, Mitchell JG, Speck PG, Newton K, Jeffries T, Paterson J. Virio-and bacterioplankton microscale distributions at the sediment-water interface. PLoS One. 2014;9(7):e102805.

[3] Grinberg M, Orevi T, Steinberg S, Kashtan N. Bacterial survival in microscopic surface wetness. eLife. 2019;8:e48508.

[4] Monier JM, Lindow SE. Frequency, size, and localization of bacterial aggregates on bean leaf surfaces. Appl Environ Microbiol. 2004;70(1):346-55.

[5] Mark Welch JL, Hasegawa Y, McNulty NP, Gordon JI, Borisy GG. Spatial organization of a model 15-member human gut microbiota established in gnotobiotic mice. PNAS. 2017;114(43):9105-14.

[6] Conwill A, Kuan AC, Damerla R, Poret AJ, Baker JS, Tripp AD, et al. Anatomy promotes neutral coexistence of strains in the human skin microbiome. Cell Host Microbe. 2022;30(2):171-82.

[7] She JJ, Liu WX, Ding XM, Guo G, Han J, Shi FY, et al. Defining the biogeographical map and potential bacterial translocation of microbiome in human 'surface organs'. Nat Commun. 2024;15(1):427.

[8] Cordero OX, Datta MS. Microbial interactions and community assembly at microscales. Curr Opin Microbiol. 2016;31:227-34.

[9] Hsu RH, Clark RL, Tan JW, Ahn JC, Gupta S, Romero PA, et al. Microbial interaction network inference in microfluidic droplets. Cell Syst. 2019;9(3):229-42.

[10] Mahrt N, Tietze A, Künzel S, Franzenburg S, Barbosa C, Jansen G, et al. Bottleneck size and selection level reproducibly impact evolution of antibiotic resistance. Nat Ecol Evol. 2021;5(9):1233-42.

[11] Wu F, Ha Y, Weiss A, Wang M, Letourneau J, Wang S, et al. Modulation of microbial community dynamics by spatial partitioning. Nat Chem Biol. 2022;18(4):394-402.

[12] Nahum JR, Godfrey-Smith P, Harding BN, Marcus JH, Carlson-Stevermer J, Kerr B. A tortoise–hare pattern seen in adapting structured and unstructured populations suggests a rugged fitness landscape in bacteria. PNAS. 2015;112(24):7530-5.

[13] Limdi A, Pérez-Escudero A, Li A, Gore J. Asymmetric migration decreases stability but increases resilience in a heterogeneous metapopulation. Nat Commun. 2018;9(1):2969.

[14] Gokhale S, Conwill A, Ranjan T, Gore J. Migration alters oscillatory dynamics and promotes survival in connected bacterial populations. Nat Commun. 2018;9(1):5273.

[15] Chakraborty PP, Nemzer LR, Kassen R. Experimental evidence that network topology can accelerate the spread of beneficial mutations. Evol Lett. 2023;7(6):447-56.

[16] Kreger J, Brown D, Komarova NL, Wodarz D, Pritchard J. The role of migration in mutant dynamics in fragmented populations. J Evol Biol. 2023;36(2):444-60.

[17] Allen B, Lippner G, Chen YT, Fotouhi B, Momeni N, Yau ST, et al. Evolutionary dynamics on any population structure. Nature. 2017;544(7649):227-30.

[18] Marrec L, Lamberti I, Bitbol AF. Toward a universal model for spatially structured populations. Phys Rev Lett. 2021;127(21):218102.

[19] Yagoobi S, Traulsen A. Fixation probabilities in network structured meta-populations. Sci Rep. 2021;11(1):17979.

[20] Abbara A, Bitbol AF. Frequent asymmetric migrations suppress natural selection in spatially structured populations. PNAS nexus. 2023;2(11):392.

[21] Verdon N, Popescu O, Titmuss S, Allen RJ. Habitat fragmentation enhances microbial collective defence. bioRxiv. 2024;2024.03.20.585867. Available from: https://www.biorxiv.org/content/early/2024/08/23/2024.03.20.585867.

[22] Fruet C, Müller EL, Loverdo C, Bitbol AF. Spatial structure facilitates evolutionary rescue by cost-free drug resistance. arXiv. 2024;2409.07377. Available from: https://arxiv.org/abs/2409.07377.

[23] Pelletier F, Garant D, Hendry HP. Eco-evolutionary dynamics. Phil Trans R Soc B. 2009;364:1483.

[24] Harrington KI, Sanchez A. Eco-evolutionary dynamics of complex strategies in microbial communities. Commun Integr Biol. 2014;7(1):e28230.

[25] Abdul-Rahman F, Tranchina D, Gresham D. Fluctuating environments maintain genetic diversity through neutral fitness effects and balancing selection. Mol Biol Evol. 2021;38(10):4362-75.

[26] Hernández-Navarro L, Asker M, Rucklidge AM, Mobilia M. Coupled environmental and demographic fluctuations shape the evolution of cooperative antimicrobial resistance. J R Soc Interface. 2023;20(208):20230393.

[27] Asker M, Hernández-Navarro L, Rucklidge AM, Mobilia M. Coexistence of Competing Microbial Strains under Twofold Environmental Variability and Demographic Fluctuations. New J Phys. 2023;25(12):123010.

[28] Hernández-Navarro L, Asker M, Mobilia M. Eco-evolutionary dynamics of cooperative antimicrobial resistance in a population of fluctuating volume and size. J Phys A: Math Theor. 2024;57(26):265003.

[29] Adamie BA, Akwar HT, Arroyo M, Bayko H, Hafner M, Harrison S, et al. Forecasting the Fallout from AMR: Economic Impacts of Antimicrobial Resistance in Food-Producing Animals. Rep EcoAMR Ser. 2024.

[30] Vollset SE, Altay U, Bhattacharjee NV, Chalek J, Giannakis K, Gray A, et al. Forecasting the Fallout from AMR: Human Health Impacts of Antimicrobial Resistance. Rep EcoAMR Ser. 2024.

[31] Naghavi M, Vollset SE, Ikuta KS, Swetschinski LR, Gray AP, Wool EE, et al. Global burden of bacterial antimicrobial resistance 1990–2021: a systematic analysis with forecasts to 2050. Lancet. 2024;404(10459):1199-226.

[32] Hengzhuang W, Wu H, Ciofu O, Song Z, Høiby N. In vivo pharmacokinetics/pharmacodynamics of colistin and imipenem in Pseudomonas aeruginosa biofilm infection. Antimicrob Agents Chemother. 2012;56(5):2683-90.

[33] Coates J, Park BR, Le D, Şimşek E, Chaudhry W, Kim M. Antibiotic-induced population fluctuations and stochastic clearance of bacteria. eLife. 2018;7:e32976.

[34] Larsson DG, Flach CF. Antibiotic resistance in the environment. Nat Rev Microbiol. 2022;20(5):257-69.

[35] Vega NM, Gore J. Collective antibiotic resistance: mechanisms and implications. Curr Opin Microbiol. 2014;21:28-34.

[36] Wahl LM, Gerrish PJ, Saika-Voivod I. Evaluating the Impact of Population Bottlenecks in Experimental Evolution. Genet. 2002;162:961.

[37] Wienand K, Frey E, Mobilia M. Evolution of a fluctuating population in a randomly switching environment. Phys Rev Lett. 2017;119(15):158301.

[38] Wienand K, Frey E, Mobilia M. Eco-evolutionary dynamics of a population with randomly switching carrying capacity. J R Soc Interface. 2018;15(145):20180343.

[39] Taitelbaum A, West R, Assaf M, Mobilia M. Population dynamics in a changing environment: random versus periodic switching. Phys Rev Lett. 2020;125(4):048105.

[40] Taitelbaum A, West R, Mobilia M, Assaf M. Evolutionary dynamics in a varying environment: Continuous versus discrete noise. Phys Rev Res. 2023;5(2):L022004.

[41] Shibasaki S, Mobilia M, Mitri S. Exclusion of the fittest predicts microbial community diversity in fluctuating environments. J R Soc Interface. 2021;18:20210613.

[42] Yurtsev EA, Chao HX, Datta MS, Artemova T, Gore J. Bacterial cheating drives the population dynamics of cooperative antibiotic resistance plasmids. Mol Syst Biol. 2013;9:683.

[43] Bush K, Bradford PA. β-Lactams and β-lactamase inhibitors: an overview. Cold Spring Harb Perspect Med. 2016;6(8):a025247.

[44] Santillan E, Seshan H, Constancias F, Drautz-Moses DI, Wuertz S. Frequency of disturbance alters diversity, function, and underlying assembly mechanisms of complex bacterial communities. NPJ Biofilms Microbi. 2019;5:1–9.

[45] Nguyen J, Lara-Gutiérrez J, Stocker R. Environmental fluctuations and their effects on microbial communities, populations and individuals. FEMS Microbiol Rev. 2021;45:fuaa068.

[46] Gude S, Pince E, Taute KM, Seinen AB, Shimizu TS, Tans JS. Bacterial coexistence driven by motility and spatial competition. Nature. 2020;578:588–592.

[47] Keymer JE, Galajda P, Muldoon C, Park S, Austin RH. Bacterial metapopulations in nanofabricated landscapes. PNAS. 2006;103(46):17290-5.

[48] Widder S, Allen RJ, Pfeiffer T, Curtis TP, Wiuf C, Sloan WT, et al. Challenges in microbial ecology: building predictive understanding of community function and dynamics. ISME J. 2016;10:2557-68.

[49] Slatkin M. Fixation probabilities and fixation times in a subdivided population. Evol. 1981;35:477-8.

[50] Keegstra JM, Carrara F, Stocker R. The ecological roles of bacterial chemotaxis. Nat Rev Microbiol. 2022;20(8):491-504.

[51] Acar M, Mettetal J, van Oudenaarden A. Stochastic switching as a survival strategy in fluctuating environment. Nat Genet. 2008;40:471-5.

[52] Lambert G, Kussell E. Memory and fintess optimization of bacteria under fluctuating environments. PLoS Genet. 2014;10(9):e1004556.

[53] Feldman WE. Concentrations of bacteria in cerebrospinal fluid of patients with bacterial meningitis. J Pediatr. 1976;88(4):549-52.

[54] Palaci M, Dietze R, Hadad DJ, Ribeiro FKC, Peres RL, Vinhas SA, et al. Cavitary disease and quantitative sputum bacillary load in cases of pulmonary tuberculosis. J Clin Microbiol. 2007;45(12):4064-6.

[55] Totlani K, Hurkmans JW, van Gulik WM, Kreutzer MT, van Steijn V. Scalable microfluidic droplet on-demand generator for non-steady operation of droplet-based assays. Lab Chip. 2020;20(8):1398-409.

[56] Goldford JE, Lu N, Bajić D, Estrela S, Tikhonov M, Sanchez-Gorostiaga A, et al. Emergent simplicity in microbial community assembly. Science. 2018;361:469.

[57] Erez A, Lopez JG, Weiner BG, Meir Y, Wingreen NS. Nutrient levels and trade-offs control diversity in a serial dilution ecosystem. eLife. 2020;9:e57790.

[58] Albright MBN, Chase AB, Martiny JBH. Experimental Evidence that Stochasticity Contributes to Bacterial Composition and Functioning in a Decomposer Community. mBio. 2019;10:e00568-19.

[59] Davies J. Inactivation of antibiotics and the dissemination of resistance genes. Science. 1994;264(5157):375-82.

[60] Wright GD. Bacterial resistance to antibiotics: enzymatic degradation and modification. Adv Drug Deliv Rev. 2005;57:1451.

[61] Bottery MJ, Wood AJ, Brockhurst MA. Selective conditions for a multidrug resistance plasmid depend on the sociality of antibiotic resistance. Antimicrob Agents Chemother. 2016;60(4):2524-7.

[62] Hughes D, Andersson DI. Selection of resistance at lethal and non-lethal antibiotic concentrations. Curr Opin Microbiol. 2012;15(5):555-60.

[63] Andersson DI, Patin SM, Nilsson AI, Kugelberg E. 21. In: The Biological Cost of Antibiotic Resistance. John Wiley & Sons, Ltd; 2007. p. 339-48.

[64] Moran PAP. The Statistical Processes of Evolutionary Theory. Oxford, UK: Clarendon; 1962.

[65] Ewens WJ. Mathematical Population Genetics. Springer, New York; 2004.

[66] van der Horst MA, Schuurmans JM, Smid MC, Koenders BB, ter Kuile BH. De novo acquisition of resistance to three antibiotics by Escherichia coli. Microb Drug Resist. 2011;17(2):141-7.

[67] Melnyk AH, Wong A, Kassen R. The fitness costs of antibiotic resistance mutations. Evol Appl. 2015;8(3):273-83.

[68] Chesson P. Mechanisms of Maintenance of Species Diversity. Annu Rev Ecol Syst. 2000;31:343.

[69] West R, Mobilia M. Fixation properties of rock-paper-scissors games in fluctuating populations. J Theor Biol. 2020;491:110135.

[70] Bena I. Dichotomous Markov noise: exact results for out-of-equilibrium systems. Int J Mod Phys B. 2006;20:2825.

[71] Horsthemke W, Lefever R. Noise-Induced Transitions. Springer, Berlin; 2006.

[72] Marrec L, Bitbol AF. Resist or perish: fate of a microbial population subjected to a periodic presence of antimicrobial. PLoS Comput Biol. 2020;16(4):e1007798.

[73] Tolker-Nielsen T, Molin S. Spatial organization of microbial biofilm communities. Microb Ecol. 2000;40:75-84.

[74] Yanni D, Márquez-Zacarías P, Yunker PJ, Ratcliff WC. Drivers of spatial structure in social microbial communities. Curr Biol. 2019;29(11):545-50.

[75] Wright S. Evolution in Mendelian populations. Genet. 1931;16(2):97.

[76] Kimura M, Weiss GH. The stepping stone model of population structure and the decrease of genetic correlation with distance. Genet. 1964;49(4):561.

[77] Gillespie DT. A general method for numerically simulating the stochastic time evolution of coupled chemical reactions. J Comput Phys. 1976;202:403.